HBRC Journal (2016) **12**, 13–24

Housing and Building National Research Center

HBRC Journal

http://ees.elsevier.com/hbrcj

A novel method to produce dry geopolymer cement powder

H.A. Abdel-Gawwad [a,*], **S.A. Abo-El-Enein** [b]

[a] *Housing and Building National Research Center, Giza, Egypt*
[b] *Faculty of Science, Ain Shams University, Cairo, Egypt*

Received 20 March 2014; revised 2 June 2014; accepted 11 June 2014

KEYWORDS

Geopolymer cement powder;
Dry activator;
Granulated blast-furnace slag;
Calcite

Abstract Geopolymer cement is the result of reaction of two materials containing aluminosilicate and concentrated alkaline solution to produce an inorganic polymer binder. The alkali solutions are corrosive and often viscous solutions which are not user friendly, and would be difficult to use for bulk production. This work aims to produce one-mix geopolymer mixed water that could be an alternative to Portland cement by blending with dry activator. Sodium hydroxide (SH) was dissolved in water and added to calcium carbonate (CC) then dried at 80 °C for 8 h followed by pulverization to a fixed particle size to produce the dry activator consisting of calcium hydroxide (CH), sodium carbonate (SC) and pirssonite (P). This increases their commercial availability. The dry activator was blended with granulated blast-furnace slag (GBFS) to produce geopolymer cement powder and by addition of water; the geopolymerization process is started. The effect of W/C and SH/CC ratio on the physico-mechanical properties of slag pastes was studied. The results showed that the optimum percent of activator and CC content is 4% SH and 5% CC, by the weight of slag, which give the highest physico-mechanical properties of GBFS. The characterization of the activated slag pastes was carried out using TGA, DTG, IR spectroscopy and SEM techniques.

Introduction

Later in 1972, Joseph Davidovits coined the name "geopolymers" [1] to describe the zeolite like polymers. Geopolymers are the alumino-silicate polymers which consist of amorphous and three dimensional structures formed from the geopolymerization of alumino-silicate monomers in alkaline solution [2]. Investigations have been carried out on calcined clays (e.g., metakaolin [3–9]) or industrial wastes (e.g., fly ash [10–14] or metallurgical slag [15,16]).

Geopolymerization is a complex process and until now it is not fully understood [17]. A reaction pathway involving the

* Corresponding author. Tel.: +20 1004540743.
E-mail address: hamdyabdelgawwad@yahoo.com (H.A. Abdel-Gawwad).
Peer review under responsibility of Housing and Building National Research Center.

Production and hosting by Elsevier

http://dx.doi.org/10.1016/j.hbrcj.2014.06.008

polycondensation of orthosialiate ions (hypothetical monomer) is proposed by Davidovits [18].

According to researchers [1,19,20], three steps are suggested in the geopolymerization process: (1) dissolution in alkaline solution; (2) reorganization and diffusion of dissolved ions with formation of small coagulated structures and (3) polycondensation of soluble species to form hydrated products. Geopolymers are well-known of their excellent properties compared to ordinary Portland cement (OPC), which are high compressive strength [21–25], low shrinkage [21,23], acid resistance [21,26], fire resistance and no toxic fumes emission [24], low thermal conductivity [21,22], excellent heavy metal immobilization [17], high temperature stability [17], low manufacturing energy consumption for construction purposes and engineering application [21], etc. They are potentially found as being used in construction engineering [17], fire proof [27], biomaterials [17], and waste treatment [17], etc. New applications are still being discovered. The geopolymerization process differs from the OPC which manufacturing involves the calcination of limestone at a high temperature with excess energy consumption and emits large amount of green house gas into the atmosphere. The production of 1 ton of OPC releases approximately 1 ton of CO_2 [28]. Thus, an alternative material was found with less energy consumption, less carbon dioxide (CO_2) emission and added with good physic-mechanical properties to solve the problem arised from OPC production. Now, it is accepted that geopolymers have emerged as an alternative to OPC.

Blended geopolymer came out by the sense to improve the porosity as well as the strength and other properties. The addition of moderate amount of calcium carbonate to a geopolymer has significant improvements on the geopolymer structure and properties [29,30].

This work aims to prepare cement powder by blending dry activator with granulated blast-furnace slag (GBFS). Formerly, geopolymer mortars and concretes were directly formed by the reaction of alumino-silicates sources with alkaline solution. Here, the alkali activator in the form of dry powder is blended with GBFS to produce blended cement powder. Sodium hydroxide (SH) reacts with calcium carbonate (CC) to produce dry activator composed of calcium hydroxide (CH), sodium carbonate (SC) and pirssonite: sodium calcium carbonate (P) according to the following equations:

$$2NaOH\,(aq.) + CaCO_3 \rightarrow Na_2CO_3 + Ca(OH)_2 \quad (1)$$

$$Na_2CO_3 + CaCO_3 + 2H_2O \rightarrow Na_2Ca(CO_3)_2 \cdot 2H_2O\,(\text{Pirssonite})) \quad (2)$$

The amount of CH, SC and P increases with the concentration of SH and consumption of CC.

There are two reasons to utilize calcium carbonate in the production of dry activator. Firstly, sodium hydroxide reacts with calcium carbonate to produce calcium hydroxide and sodium carbonate and pirssonite Eqs. (1) and (2) and secondly, the remaining calcium carbonate from the reaction acts as a filler material which decreases porosity and increases the compressive strength of activated slag [29,30].

This process was investigated in this work to produce blended cement powder. The important parameters involved in the blended cement powder are SH concentration, SH:CC ratio, and (W/C) ratio. This blended cement powder, if succeeded, could be an alternative to OPC which can be used to produce mortar and concrete by addition of small amounts of water.

Experimental

Materials

Granulated blast-furnace slag (GBFS) was purchased from Helwan Steel Company, Egypt. Calcium carbonate was obtained from Arabic Chemical Company. Sodium hydroxide (SH) powder of 99% purity was obtained from Fisher Scientific Company.

The chemical composition of granulated blast furnace slag and calcium carbonate as determined by X-ray Fluorescence (XRF) is seen in Table 1. Fig. 1a and b shows the mineralogical composition of GBFS and CC. Particle size analysis of dry activator (DA) and GBFS using a Coulter LS130 optical size analyzer is shown in Fig. 2.

Blended cement powder synthesis

The Granulated blast furnace slag (GBFS) was first passed through a magnet to remove any contamination of iron and then ground in a steel ball mill. Alkali activator (SH) solution was mixed with calcium carbonate (CC^{-}) powder and dried in an oven at 80 °C for 8 h then followed by pulverization to a fixed particle size to produce the dry activator powder. The activator was blended with GBFS. The details of mix proportions of blended cement powders are shown in Table 2.

Preparation of cement pastes

Each blended cement powder was placed on smooth, non absorbent surface, a crater was formed in the centre and water was poured into the crater. The dry mixture was slightly toweled over the remaining mixture to absorb the water for about one minute. The mixing operation was then completed by continuous and vigorous mixing by means of an ordinary gauging trowel for about three minutes. The paste was placed in one cubic inch moulds and manually pressed strongly at the corner along the surface of the mould. After compaction of the top layer, the surface of the paste was smoothed by a thin edged trowel. The hardened slag pastes were cured in 100% relative humidity at 37 ± 2 °C up to 28 days.

Characterization methods

Compressive strength

This test was carried out on four specimens according to ASTM C109 M [31]; the surface of the specimens was carefully polished on fine paper in order to remove irregularities. To help transmit the load to the specimen's faces uniformly pieces of cardboard 2 mm in thickness were placed on both faces. Compressive strength measurements were carried out using a five tonne German Brüf Pressing Machine with a loading rate of 100 kg/min.

Water absorption

The water absorption measurements, ASTM C1403-13 [32], were done by weighing the saturated specimens (W1) and dried

Table 1 Chemical compositions of calcium carbonate (CC) and granulated blast-furnace slag (GBFS), wt.%.

Oxide (%)	SiO_2	Al_2O_3	Fe_2O_3	CaO	MgO	Na_2O	K_2O	SO_3	TiO_2	P_2O_5	L.O.I	Total
CC^-	0.09	0.03	–	55.91	0.08	–	0.18	0.1	–	0.03	43.64	99.99
GBFS	37.81	13.14	0.23	38.70	7.11	1.03	0.19	1.19	0.40	0.17	–	99.97

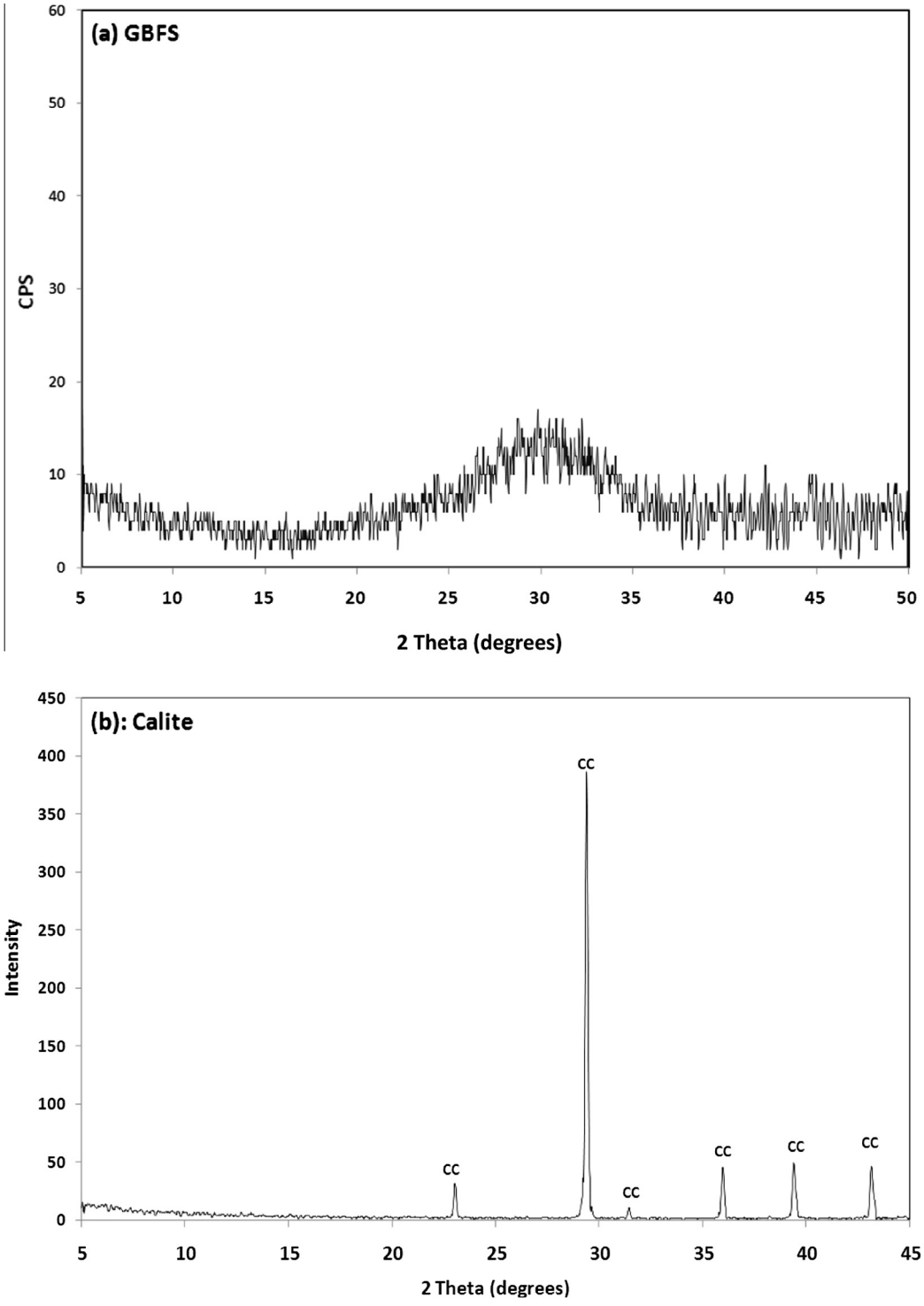

Fig. 1 XRD patterns of (a) slag and (b) calcite.

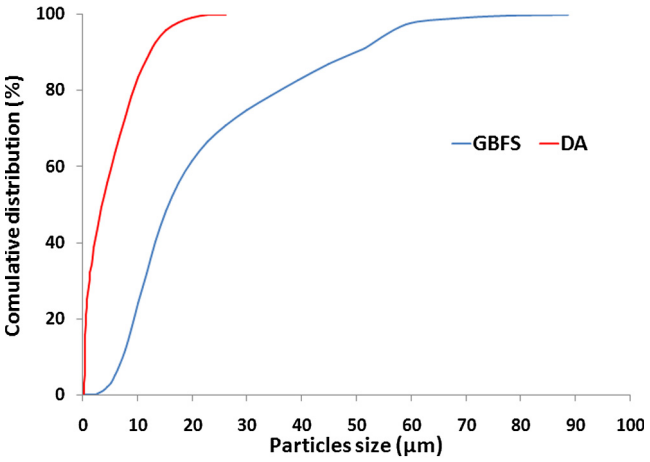

Fig. 2 Particle size distribution of granulated blast furnace slag (GBFS) and dry activator powder (DA).

specimens in an oven at 80 °C for 24 h (W2) after 3, 7, 14 and 28 days. The water absorption is calculated from the following equation:

$$\text{Water absorption}\% = [(W1 - W2)/W1] \times 100.$$

Setting time

The initial and final setting times were both measured using the Vicat test according to ASTM C191-13 [33].

X-ray diffraction (XRD)

The crystalline phases in the prepared samples and mixes were identified using the X-ray diffraction technique. Nickel-filtered Cu-kα radiation at 40 kV and 20 mA was used throughout a Philips PW3050/60 diffractometer, provided with a proportional counter.

Thermal analysis (DTA/TGA)

Differential thermal analysis (DTA) and thermogravimetric analysis (TGA) were carried out by heating the sample in nitrogen atmosphere up to 1000 °C at a heating rate of 20 °C/min using a DT-50 Thermal Analyzer (Schimadzu Co-Kyoto, Japan). The results were compared with DTA standard data.

Fourier transforms infrared spectroscopy (FTIR)

Infrared spectra were recorded from 4000 cm^{-1} to 400 cm^{-1} using Perkin Elmer FTIR Spectrum RX1 Spectrometer.

Scanning electron microscopy (SEM)

The scanning electron microphotographs were obtained with Inspect S (FEI Company, Holland) equipped with an energy dispersive X-ray analyzer (EDXA).

Results and discussion

Characterization of dry activator powder

The DTA thermograms of CC and dry activators (NC9, NC14, and NC19) are shown in Fig. 3a. The endothermic peaks located at 441, 460 and 470 °C are related to dehydroxylation of CH; endothermic peak located in the range of 104–187 °C is related to the removal of combined water of pirssonite (P). Endotherms located at 782–862 °C are due to the decomposition of sodium and calcium carbonates. Fig. 3b shows XRD diffractograms of calcium carbonate (CC) and dry activator powders (NC9, NC14, NC19); the intensities of CH, SC and P peaks increase from NC9 NC14 and NC9. This is due to that the amount of calcium carbonate decreases in the opposite direction as shown in Table 2.

Setting time

The initial and final setting times of GBFS blended with dry activators (NC12, NC14 or NC16) are shown in Fig. 4a. The initial and final setting times of GBFS-NC16 (C) are shorter than those of GBFS-NC14 (B) or GBFS-NC12 (A) pastes. This is due to that the higher content of SC and CH tends to increase the liberation of Ca^{2+}, Si^{4+} and Al^{3+} from the slag grains and consequently increases the geopolymerization rate. This is due to that the calcium hydroxide in dry activators acts as an accelerator for the hydration reaction leading to form more hydration products and therefore shorten the setting times. Also, the setting times of GBFS-NC19 paste are shorter than those of GBFS-NC14 (B) or GBFS-NC9 (G) pastes. This is attributed to higher CC/SH ratio of NC19 than those of NC14 or NC9 dry activators. The calcium carbonate acts as a nucleating site then increases with the amount of calcium carbonate, leading to the formation of more hydration products. As the amount of hydrated material increases, the number of contact points between the hydration products also increases, eventually establishing a solid microstructure [34]. On the other side, Fig. 4b shows that the initial and final setting times of slag activated by sodium hydroxide (GBFS-SH, I) are longer than those GBFS-NC9 (G), GBFS-NC14 (B) or GBFS-NC19 (H) blends.

Table 2 Mixed composition of blended slag cement pastes.

Mix symbol	Dry activator designation	SH,%	CC,%	GBFS,%	W/C ratio
A	NC12	2	10	88	0.27
B	NC14	4	10	86	0.27
C	NC16	6	10	84	0.27
D	NC14	4	10	86	0.24
E	NC14	4	10	86	0.30
F	NC14	4	10	86	0.33
G	NC9	4	5	91	0.27
H	NC19	4	15	81	0.27
I	–	4	0	96	0.27

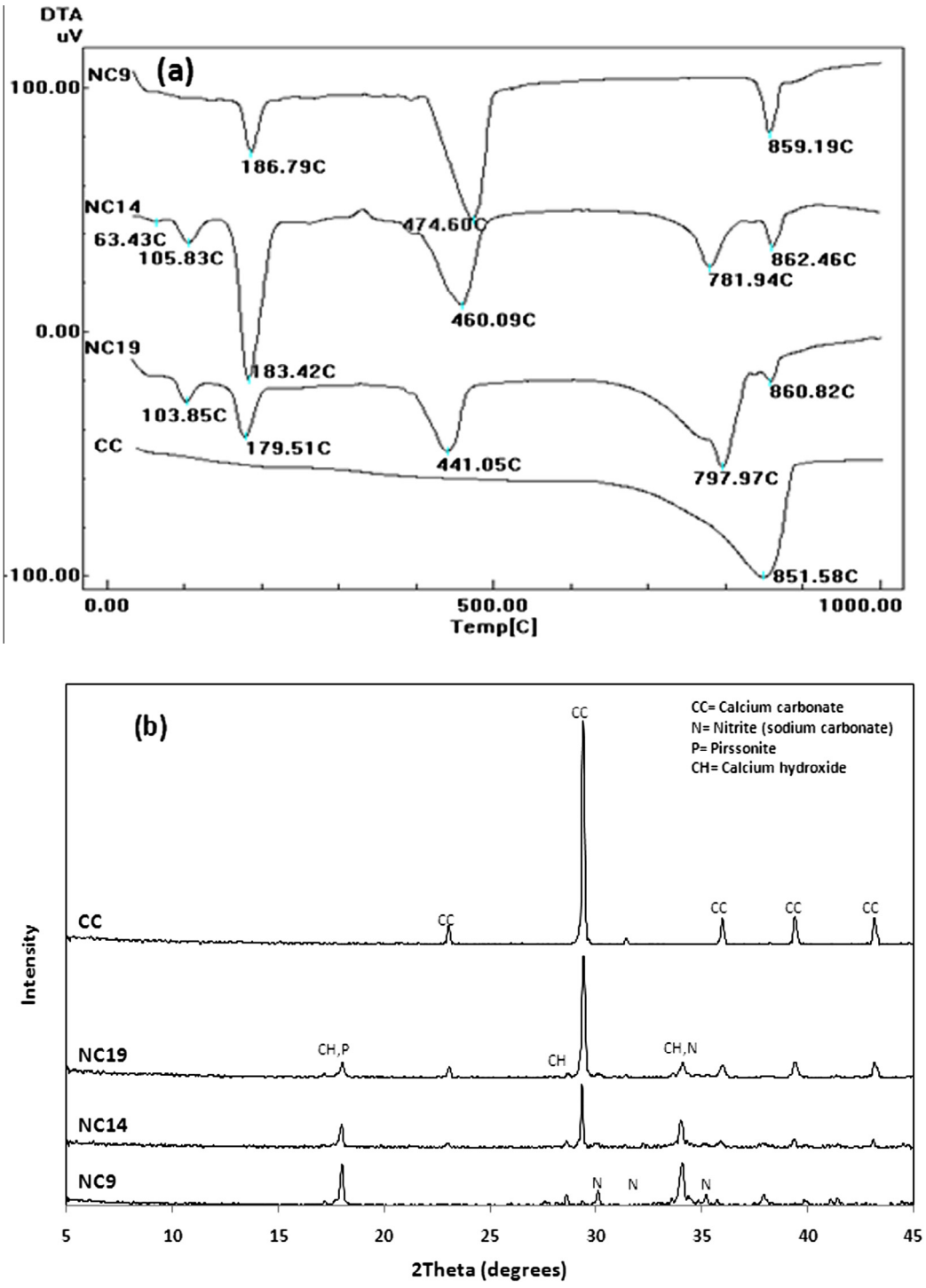

Fig. 3 (a) DTA thermograms and (b) XRD diffractograms of calcium carbonate (CC^{-}) and dry activators (NC9, NC14 and NC19).

Water absorption

It is clear that the water absorption values of slag cement pastes (A, B and C) with dry activators NC12, NC14 or NC16, as shown in Fig. 5a, decrease with NC12 up to NC14 followed by a slight increase with NC16. This is due to that with the increase of SC and CH concentrations the rate of geopolymer formation increases, until a maximum is reached, and then the rate is reduced by additional SC and CH [35].

Fig. 5b presents the water absorption values of GBFS-NC14(B) blend at different W/C ratios of 0.24, 0.27, 0.30 and 0.33. Evidently, the water absorption values decrease with the W/C ratio from 0.24 to 0.27 then increase from 0.27 up to 0.33. This is due to that with the increase of W/C ratio from

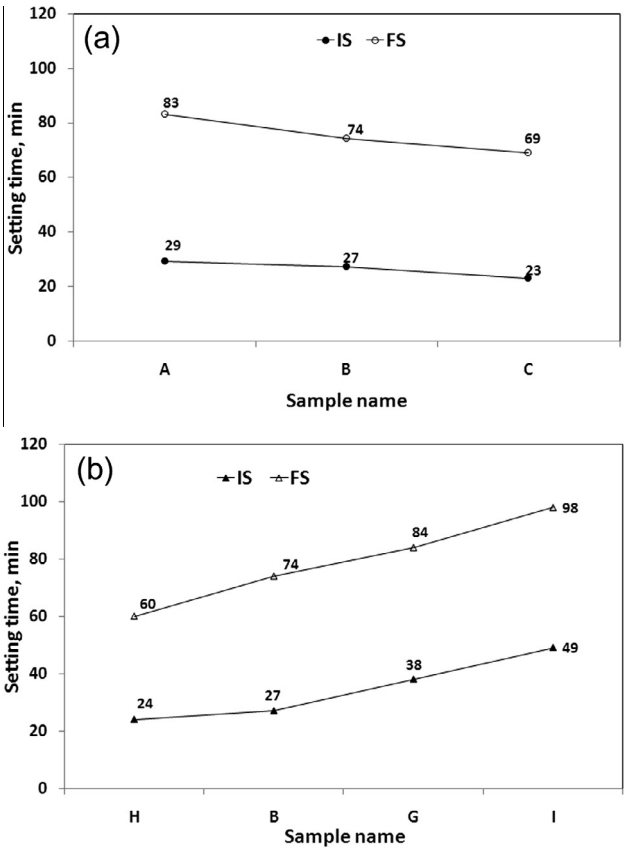

Fig. 4 Initial and final setting times of (a) GBFS-NC12 (A), GBFS-NC14 (B) and GBFS-NC16 (C) blends and (b) GBFS-NC9 (G), GBFS-NC14 (B), GBFS-NC19 (H) and GBFS-SH (I) blends.

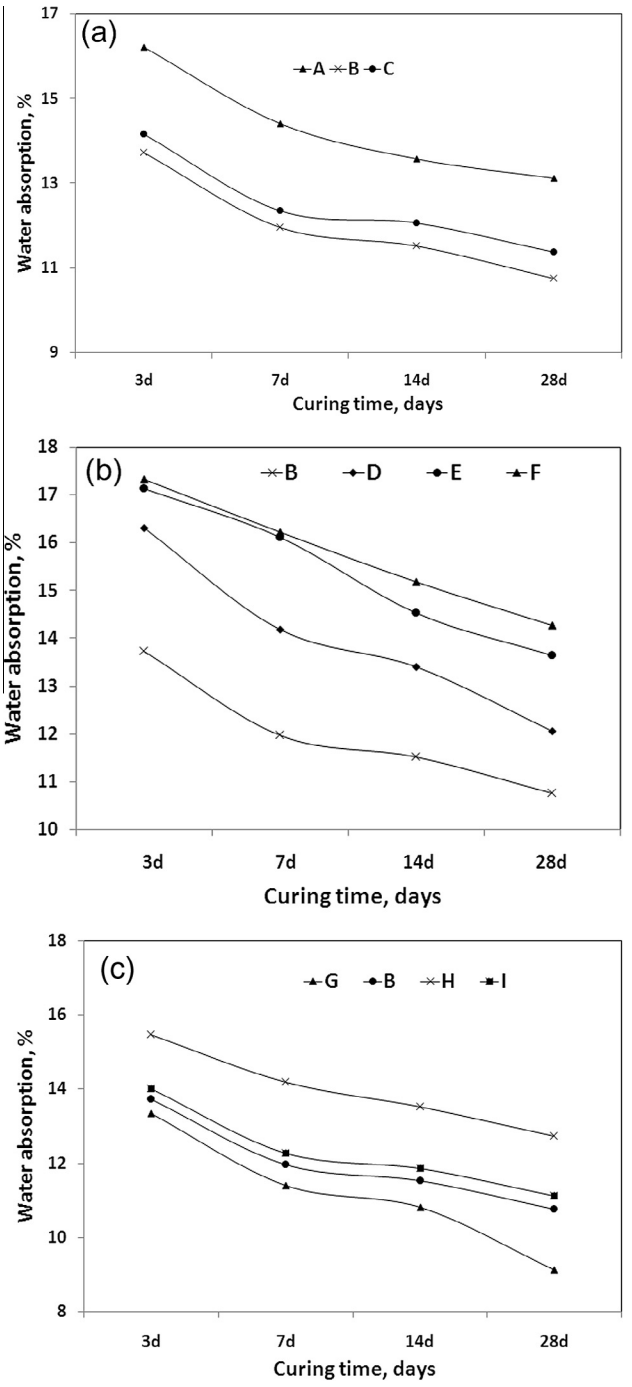

Fig. 5 Water absorption of (a) GBFS-NC12 (A), GBFS-NC14 (B) and GBFS-NC16 (C) blends,(b) GBFS-NC14 at different W/C ratios of 0.24 (D), 0.27 (B), 0.30 (E) and 0.33 (F) and (c) GBFS-NC9 (G), GBFS-NC14(B), GBFS-NC19 (H) and GBFS-SH (I) blends at 28 days of curing.

0.24 to 0.27 the mobility of sodium and calcium ions enhances leading to an increase in the geopolymerization rate. However, with further increase in W/C from 0.27 to 0.33 the porosity of cement matrix increases with a consequent increase of the water absorption values.

Fig. 5c illustrates the water absorption of slag cement activated by sodium hydroxide(I) and slag pastes (G, B, H) blended with dry activator (NC9, NC14 or NC19). The water absorption values of GBFS activated by SH (I) are higher than those of GBFS-NC14 (B) or GBFS-NC9 (G) pastes. This result is mainly related to, the amount of finely ground carbonates (SC and CC) present in NC9 and NC14 which act as a filler material leading to decrease in pore size and, then the water absorption [30]. On the other side, the water absorption values of slag pastes with dry activators (NC9, NC14 or NC19) increase from NC9 up to NC19. This is due to that the calcium carbonate content increases from NC9 to NC19 which reduces the reactive aluminosilicate content [29].

Compressive strength

The compressive strength values of slag pastes (A, B and C) with dry activator (NC12, NC14 or NC16) are given in Fig. 6a. The compressive strength of granulated slag blended with dry activator NC14 is greater than that with NC12 or NC16. The alkali activators are known to speed the dissolution of aluminosilicate in water [35]. Faster dissolution releases higher concentrations of silicate, aluminate, and/or aluminosilicate species into solution. This may appear to imply faster geopolymer network formation, due to rapid GBFS destruction; however, this is not necessarily the case. Although the increase of sodium hydroxide did shorten the induction period, the rate of network formation after this period was not always increased. This indicates that the rate determining step is likely

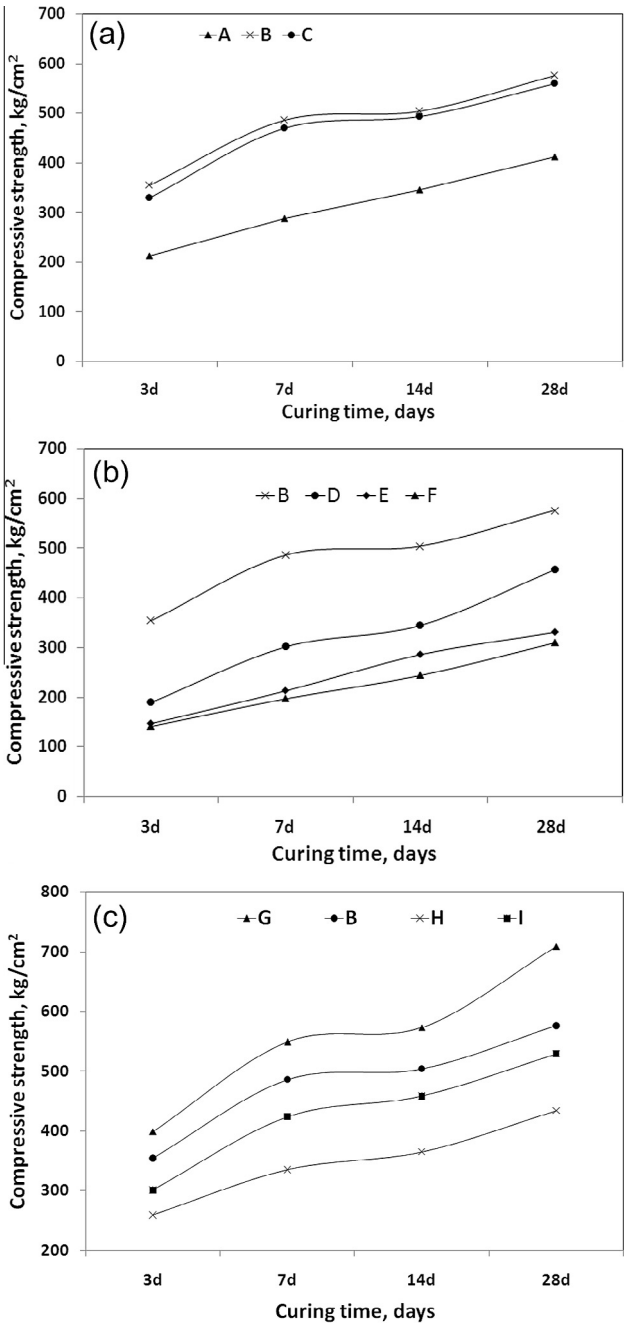

Fig. 6 Compressive strength versus curing time for (a) GBFS-NC12 (A), GBFS-NC14 (B) and GBFS-NC16 (C) blends,(b) GBFS-NC14 at different W/C ratios of 0.24 (D), 0.27 (B), 0.30 (E) and 0.33 (F) and (c) GBFS-NC9 (G), GBFS-NC14(B), GBFS-NC19 (H) and GBFS-SH (I) blends at 28 days of curing.

to be geopolymer network formation rather than GBFS hydrolysis, and network formation is less favored at high pH due to the redissolution of gel component.

Fig. 6b shows the effect of W/C ratio (0.24, 0.27, 0.30 and 0.33 for mixes D, B, E, and F, respectively) on the compressive strength of GBFS-NC14 paste. It was found that the compressive strength increases with W/C ratio to 0.27 then decreases to 0.33. With increase in the mixing water up to 0.27 W/C ratio, the solubility of dry activator increases which leads to an enhancement in the rate of geopolymerization and, therefore, a consequent increase in the compressive strength. However, when, the W/C ratio increases from 0.27 to 0.33, the porosity of cement matrix increases and, then the compressive strength decreases. The optimum W/C ratio required for the GBFS-NC14 paste is 0.27.

Fig. 6c shows the compressive strength of GBFS paste activated by sodium hydroxide (I) and the pastes (G, B and H) activated with dry activators (NC9, NC14 and NC19), respectively. The compressive strength values of slag pastes activated by sodium hydroxide are lower than those GBFS-NC9 (G) or GBFS-NC14(B) pastes at all ages. Obviously, the slag pastes activated by dry activators or sodium hydroxide have the same content of sodium oxide, while the second has an additional quantity of calcium hydroxide which is produced from the reaction of sodium hydroxide and calcium carbonate Eqs. (1) and (2). This calcium hydroxide accelerates the geopolymerization and pozzolanic reaction to form more geopolymer and hydration products. On the other side, the carbonates (carbonate from calcium and sodium carbonate) in dry activators (NC14, NC9) act as filler material which reduced the pore sizes of cement paste and consequently decrease the water absorption as well as increase the compressive strength. The compressive strength of slag blended with NC9 is higher than those with NC14 and NC19 at all ages of hydration. This is attributed to the reduction of aluminosilicate by addition of calcium carbonate.

FTIR spectroscopy

Fig. 7a shows the FTIR-spectra of anhydrous GBFS, hardened pastes of GBFS–NC12 (A), GBFS-NC14 (B) and GBFS-NC16(C) after 28 days in 100% relative humidity. The results indicate different absorption bands. The absorption band at 464–492 cm^{-1} is due to O–Si–O bonds bending vibration, the bands typical of carbonate phases are seen: at 876, 1423, 1485, 1426 and 1424 cm^{-1}. These bands are connected with the presence of $CaCO_3$ and Na_2CO_3. The carbonate band intensity of GBFS-NC12 (A) is more intense than those of GBFS-NC14 (B) and GBFS-NC16 (C). This is attributed to that the CC/SH ratio in the dry activator (NC12) is greater than those of NC14 or NC16. Additionally, a relatively well resolved band at 653–717 cm^{-1} appeared which is associated to the symmetric stretching vibrations of Si–O–Al bridges. The absorption band located at 1631–1637 cm^{-1} is due to bending H–O–H vibration and the absorption band at 3436–3452 cm^{-1} is due to stretching of O–H groups; This band disappeared in anhydrous GBFS due to the absence of hydration products such as C–S–H or C–A–H. The absorption bands of water are an indication to crystalline H_2O of the hydrated products such as C–S–H and C–A–H [35]. The absorption bands located at 988–970 cm^{-1} are due to Si (Al)–O asymmetric stretching vibrations. The high full width at half maximum (FWHM) of this band of anhydrous GBFS is wider than that of GBFS-dry activator blends. It is known that phases of non-ordered structure increase the band width due to the existence of significant fluctuations of geometric parameters, i.e., bond lengths and angles [36]. The intensity of the bands at 1637, 3452 cm^{-1} for GBFS-NC14 (B) is bigger than those obtained for the GBFS-NC12 (A). This is due to the higher CH content of NC14 dry activator than that of NC12 which accelerates the

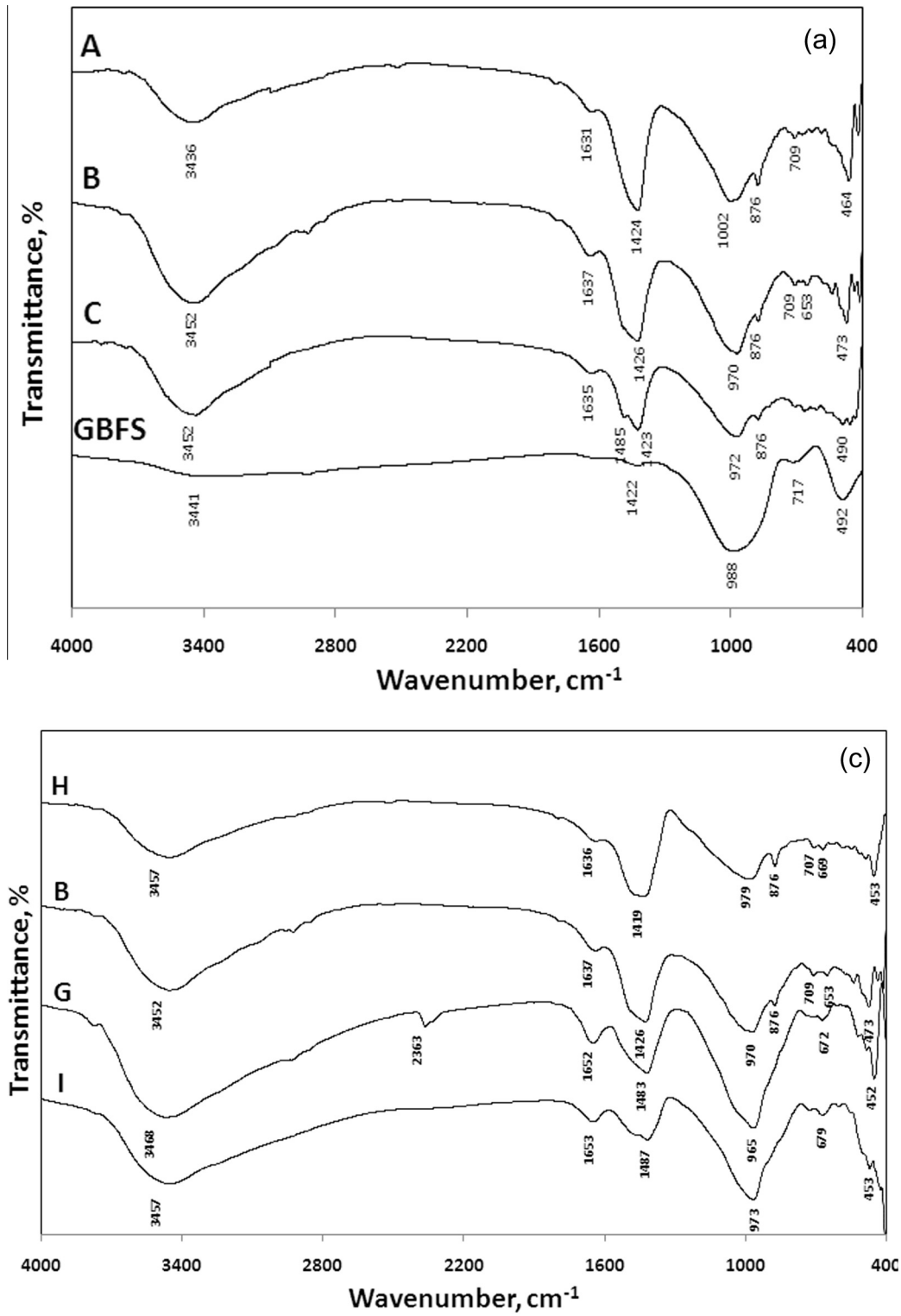

Fig. 7 FTIR spectra of (a) GBFS-NC12 (A), GBFS-NC14 (B) and GBFS-NC16 (C) and (b) GBFS-NC9 (G), GBFS-NC14(B), GBFS-NC19 (H) and GBFS-SH (I) blends at 28 days of curing.

hydration reaction leading to form more hydration products (C–S–H and C–A–H). On the other side, the NC14 has more sodium oxide content than that of NC12 which is responsible for dissolution of slag network forming Si^{4+}, Al^{3+} and Ca^{2+} ions and, therefore, forming C–S–H and C–A–H. Although the NC16 has more sodium carbonate and calcium hydroxide contents, the intensity of bands related to C–S–H, C–A–S–H and Si (Al)–O decreases. This is mainly due to that the

geopolymerization rate and pozzolanic reactions increase with the amounts of SC and CH until maximum is reached, then reduced by additional alkalis.

Fig. 7b presents the FTIR-spectra of GBFS activated by sodium hydroxide (I), hardened paste-dry activator of GBFS-NC9 (G), GBFS-NC14 (B) and GBFS-NC19 (H) after 28 days of curing in 100% RH. Absorption bands obtained for GBFS-NC9 paste (G) which is related to O–Si–O bond bending vibration, symmetric stretching vibrations of the Si–O–Si(Al) bridges, Si (Al)–O anti symmetric stretching vibrations, bending H–O–H vibration, and stretching of O–H groups, appeared at 452, 672, 711, 965, 1652, 2363 and 3468 cm^{-1}, are more intense than those obtained for the GBFS activated by SH. This is mainly due to that the CH content in dry activator (NC9) accelerates the geopolymerization as well as pozzolanic reaction which leads to form more geopolymer and hydration products. On the other side, the intensity of absorption bands of GBFS-NC19 (H) which is related to carbonate is higher than those of GBFS-NC14 (B), GBFS-NC9 (H) pastes and GBFS activated by SH. This is attributed to that the higher CC/SH ratio causes the decrease of aluminosilicate content of GBFS leading to a decrease in the intensities of bands of geopolymers (O–Si–O bond bending vibration, symmetric stretching vibrations of the Si–O–Si(Al) bridges, Si (Al)–O anti symmetric) and hydration products (bending H–O–H vibration, and stretching of O–H groups). The intensity of bands related to O–Si–O bond bending vibration, symmetric stretching vibrations of the Si–O–Si(Al) bridges, anti symmetric stretching vibrations Si (Al)–O of GBFS activated by SH (I) is higher than those of GBFS-NC14 (B) while the intensity of bands related to bending H–O–H vibration, and stretching of O–H groups of GBFS-NC14 is higher than those of GBFS activated by SH. This is due to that the calcium carbonate in dry activator (NC14) reduces the aluminosilicate content while calcium hydroxide in dry activator acts as a calcium ion source which accelerates the pozzolanic reaction leading to form more hydration products (C–S–H and C–A–S–H).

In conclusion, the results of infrared spectra obtained for slag cement pastes are in agreement with those of compressive strength of the hardened pastes.

Thermogravimetric analysis

Fig. 8a presents TGA and DTG thermograms of GBFS-NC12 (A), GBFS-NC14 (B) and GBFS-NC16 (C) pastes after 28 days in 100% RH. The weight loss due to the decomposition of hydrated products was determined from the TGA thermograms. The weight loss at 1000 °C was found to be 9.18%, 12.95% and 11.82% for mixes A, B and C, respectively. The endotherm characteristic for each hydrated product could be distinguished by DTG. The endothermic peaks located at 50–200 °C are related to dehydration of calcium silicate hydrate (C–S–H) and calcium aluminate silicate hydrate (C–A–S–H) [37]. The endothermic peak located at 733–739 °C is due to the decomposition of calcium carbonate. Obviously, the weight loss of GBFS-NC14 (B) paste is greater than those of GBFS-NC12 (A) and GBFS-NC16 (C) pastes, respectively. This is due to that the amount of CSH formed in GBFS-NC14 (B) paste is greater than those of GBFS-NC12 (A) and GBFS-NC16 (C). On the other hand, the intensity of the endotherm characteristic for calcium carbonate in case of GBFS-NC12

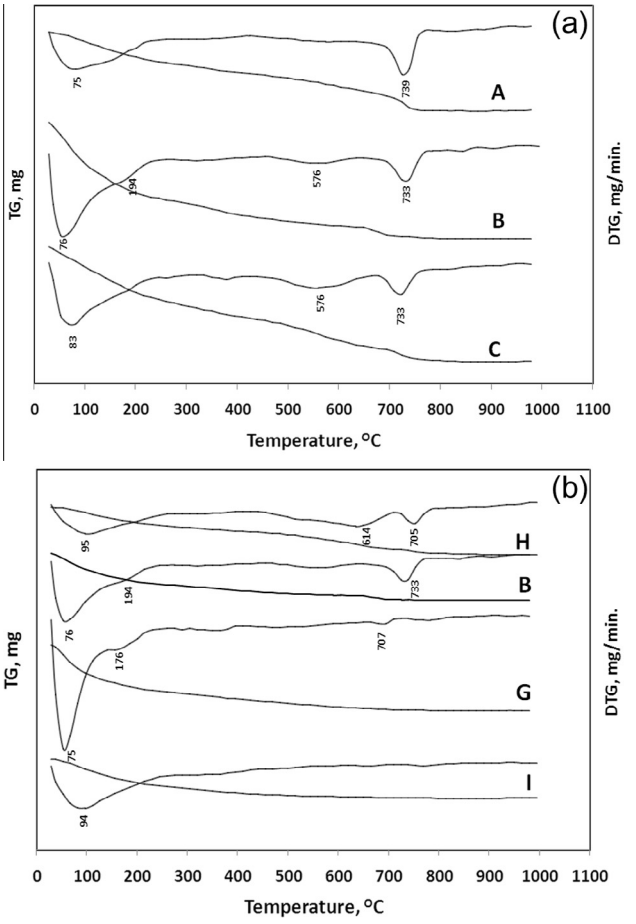

Fig. 8 TGA, DTG thermograms of (a) GBFS-NC12 (A), GBFS-NC14 (B) and GBFS-NC16 (C) and (b) GBFS-NC9 (G), GBFS-NC14(B), GBFS-NC19 (H) and GBFS-SH (I) blends at 28 days of curing.

(A) is higher than those of GBFS-NC14 (B) and GBFS-NC16 (C). This result is mainly related to the value of CC^{-}/SH ratio of the activator; this ratio decreases in order NC12 > NC14 > NC16.

Fig. 8b shows TGA and DTG thermograms for GBFS activated by sodium hydroxide (I), GBFS-NC9 (G), GBFS-NC14 (B) and GBFS-NC19 (H) after 28 days in 100% RH. The weight loss of GBFS-NC9 (G) paste (16.51%) is greater than those of GBFS-NC14 (B) paste, GBFS-NC19 (H) paste and GBFS activated by sodium hydroxide (I) (12.95 and 14.05, 10.18%), respectively. This is due to that the amount of CSH formed in GBFS-NC9 (G) paste is greater than those of GBFS-NC14 (B) and GBFS-NC19 (H) pastes. Although the CSH formed in GBFS-NC19 (H) blend is lower than those formed in GBFS-NC14 (B) paste or GBFS activated by sodium hydroxide (I), the weight loss for GBFS-NC19 (H) paste is greater than those of GBFS-NC14 (B) paste or GBFS activated by sodium hydroxide (I). The weight loss of GBFS-NC19 paste (H) is greater than that of GBFS-NC14 paste (B) and GBFS activated by sodium hydroxide (I); this is mainly due to that the GBFS-NC19 (H) blend has a high amount of calcium carbonate than those of GBFS-NC14 (B) paste or GBFS activated by sodium hydroxide (I) as indicated from the DTG thermograms.

Scanning electron microscopy (SEM)

Fig. 9 presents the scanning electron micrographs obtained for the hardened pastes of GBFS activated by sodium hydroxide, GBFS-NC9 blend (G) and GBFS-NC19 blend (H), at two magnifications (a) 300 μm and (b) 50 μm), for 28 days. It is clear that the micrograph of hardened paste of GBFS-NC9 blend (G) is highly homogeneous and more dense with compact microstructure as compared to GBFS-NC19 (H) or GBFS activated by sodium hydroxide (I). Also, the content of calcium silicate hydrate (CSH) formed in GBFS-NC9 (G) blend is greater than that formed in GBFS activated by sodium hydroxide (I). The morphology of CSH formed in GBFS-NC9 blend differed from that formed in case of GBFS activated by sodium hydroxide. This is mainly due to different Ca^{2+}/Si^{4+} ratio. Calcium carbonate distributed along hardened paste of GBFS-NC19 was observed. The open pores (P) that appeared in case of GBFS-NC19 are due to the higher CC^{-}/SH ratio which reduces the aluminosilicate content leading to a decrease in geopolymerization and pozzolanic reaction rates and, therefore, decreases the compressive strength and increases the water absorption. The dense and compact microstructure of

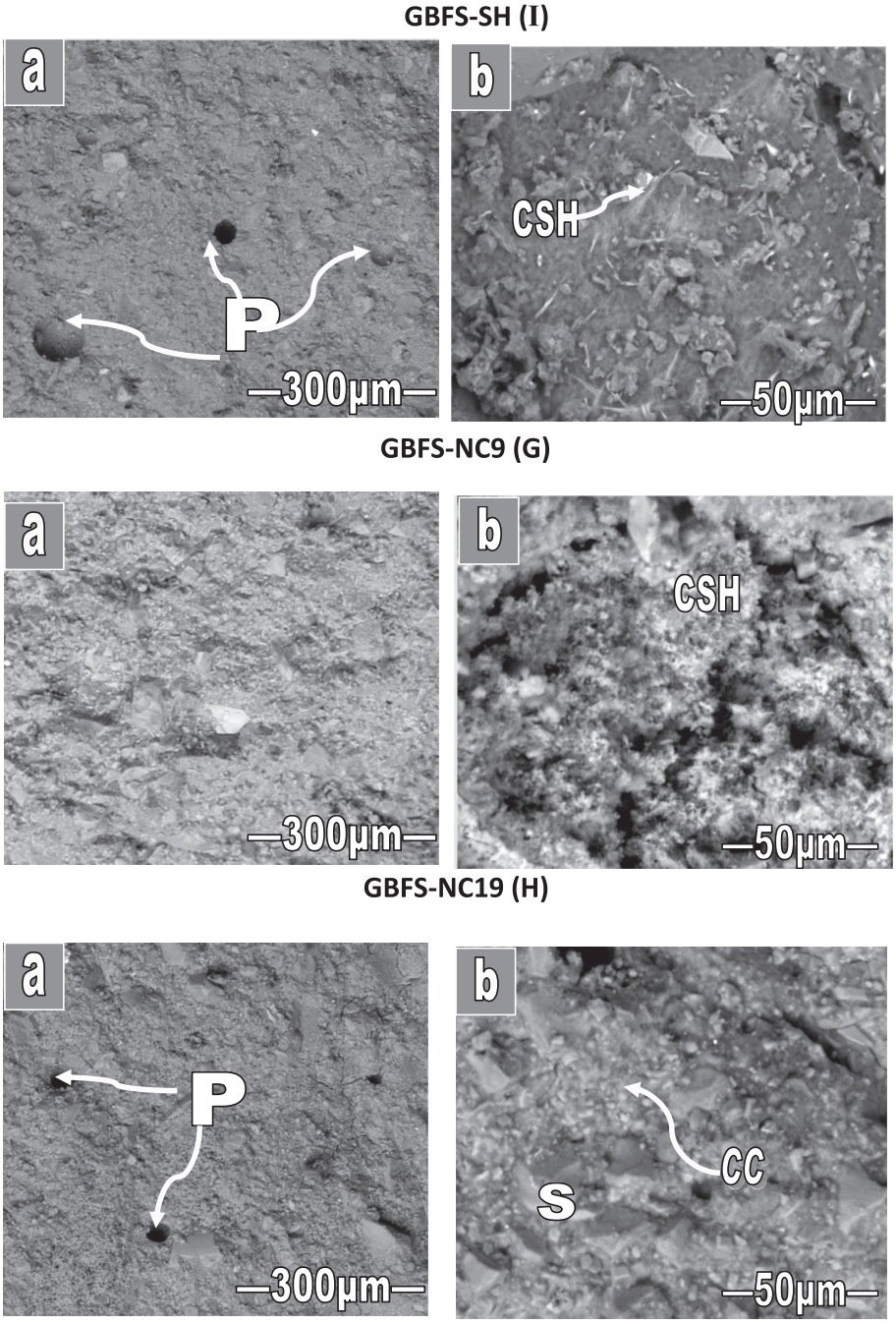

Fig. 9 SEM micrographs of GBFS-SH, GBFS-NC9 and GBFS-NC19 blend at 28 days of curing.(S, unreacted slag; CC, calcium carbonate; P, open pores; CSH, calcium silicate hydrate).

GBFS-NC9 as a result of relatively lower CC^{-}/SH ratio in dry activator (NC9) of mix G which leads to the dissolution of activated species (Al^{3+}, Si^{4+} and Ca^{2+}) is sufficient for the formation of geopolymer and hydrated product (CSH), thus, producing a very compact structure.

The SEM observations are in agreement with those of water absorption, compressive strength, FTIR spectra, TGA and DTG analyses.

Conclusion

The main findings of this study can be summarized as follows:

(i) XRD and DTA show that the dry activator composes sodium carbonate, calcium hydroxide, pirssonite and calcium carbonate.
(ii) The higher compressive strength and lower water absorption were obtained by blending GBFS with NC9 dry activator at W/C ratio of 0.27.
(iii) FTIR spectra showed the band characteristic for geopolymer bonding (Al–O–Si and Si–O–Si) and calcium silicate hydrate. The intensity of these bands depends primarily on the composition of dry activator.
(iv) TGA/DTG analyses showed that the intensity of the endotherm of calcium silicate hydrate depends on the dry activator composition.
(v) SEM micrographs have proved that the dry activator plays an important role in the geopolymerization process then continued after addition of water to form a more homogeneous structure.
(vi) Finally, the physico-mechanical properties of GBFS activated with dry activators (NC9 and NC14) are higher than those of activated by sodium hydroxide.

References

[1] K. Komnitsas, D. Zaharaki, Geopolymerisation: a review and prospects for the minerals industry, Miner. Eng. 20 (2007) 1261–1277.
[2] M. Rowles, B. O'Connor, Chemical optimization of the compressive strength of aluminosilicate geopolymers synthesized by sodium silicate activation of metakaolinite, J. Mater. Chem. 13 (2003) 1161–1165.
[3] Y.S. Zhang, W. Sun, L. Zongjin, Composition design and microstructural characterization of calcined kaolin-based geopolymer cement, Appl. Clay Sci. 47 (2010) 271–275.
[4] W. Sun, Zhang Yun-sheng, Lin Wei, Liu Zhi-yong, In situ monitoring of the hydration process of K-PS geopolymer cement with ESEM, Cem. Concr. Res. 34 (2004) 935–940.
[5] M. Murat, Hydration reaction and hardening of calcined clays and related minerals: II. Influence of mineralogical properties of the raw-kaolinite on the reactivity of metakaolinite, Cem. Concr. Res. 13 (4) (1983) 511–518.
[6] R. Cioffi, L. Maffucci, L. Santoro, Optimization of geopolymer synthesis by calcination and polycondensation of a kaolinitic residue, Resour. Conserv. Recycl. 40 (2003) 27–38.
[7] H. Wang, H. Li, F. Yan, Synthesis and mechanical properties of metakaolinite based geopolymer, Colloids Surf. 268 (2005) 1–6.
[8] P. Duxson, S.W. Mallicoat, G.C. Lukey, W.M. Kriven, J.S.J. van Deventer, The effect of alkali and Si/Al on the development of mechanical properties of metakaolin-based geopolymers, Colloids Surface A: Physicochem. Eng. Aspects 292 (2007) 8–20.
[9] D.L.Y. Kong, J.G. Sanjayan, K. Sagoe-Crentsil, Comparative performance of geopolymers made with metakaolin and fly ash after exposure to elevated temperatures, Cem. Concr. Res. 37 (2007) 1583–1589.
[10] E.I. Diaz, E.N. Allouche, S. Eklund, Factors affecting the suitability of fly ash as source material for geopolymers, Fuel 89 (2010) 992–996.
[11] D.L.Y. Kong, J.G. Sanjayan, Effect of elevated temperatures on geopolymer paste, mortar and concrete, Cem. Concr. Res. 40 (2010) 334–339.
[12] X. Guo, H. Shi, W.A. Dick, Compressive strength and microstructural characteristics of class C fly ash geopolymer, Cem. Concr. Compos. 32 (2010) 142–147.
[13] J. Temuujin, A. van Riessen, Effect of fly ash preliminary calcination on the properties of geopolymer, J. Hazard. Mater. 164 (2009) 634–639.
[14] J. Temuujin, A. van Riessen, K.J.D. MacKenzie, Preparation and characterisation of fly ash based geopolymer mortars, Constr. Build. Mater. 24 (2010) 1906–1910.
[15] Zhang Yunsheng, Sun Wei, Chen Qianli, Chen Lin, Synthesis and heavy metal immobilization behaviours of slag based geopolymer, J. Hazard. Mater. 143 (2007) 206–213.
[16] J.J. Chang, A study on the setting characteristics of sodium silicate-activated slag pastes, Cem. Concr. Res. 33 (2003) 1005–1011.
[17] Xiao Yao, Zuhua Zhang, Huajun Zhu, Yue Chen, Geopolymerization process of alkali-metakaolinite characterized by isothermal calorimetry, Thermochim. Acta 493 (2009) 49–54.
[18] J. Davidovits, Geopolymers: inorganic polymeric new materials, J. Therm. Anal. 37 (1991) 1633–1656.
[19] D. Dimas, L. Giannopoulou, D. Panias, Polymerization in sodium silicate solutions: a fundamental process in geopolymerization technology, J. Mater. Sci. 44 (2009) 3719–3730.
[20] S. Alonso, A. Palomo, Calorimetric study of alkaline activation of calcium hydroxide-metakaolin solid mixtures, Cem. Concr. Res. 31 (1) (2001) 25–30.
[21] Yao Jun Zhang, Ya Chao Wang, De Long Xu, Sheng Li, Mechanical performance and hydration mechanism of geopolymer composite reinforced by resin, Mater. Sci. Eng. 527 (2010) 6574–6580.
[22] P. Duxson, A. Fernández-Jiménez, J.L. Provis, G.C. Lukey, A. Palomo, J.S.J. van Deventer, Geopolymer technology: the current state of the art, J. Mater. Sci. 42 (2007) 2917–2933.
[23] Chi Mao-chieh, Chang Jiang-jhy, Huang Ran, Strength and drying shrinkage of alkali-activated slag paste and mortar, Adv. Civ. Eng. 2012 (2012). Article ID 579732.
[24] Peter Duxson, L. John, Provis, C. Grant, Lukey, S.J. van Deventer Jannie, The role of inorganic polymer technology in the development of 'Green Concrete', Cem. Concr. Res. 37 (2007) 1590–1597.
[25] O.R.X. Burciaga-Díaz, Magallanes-Rivera, J.I. Escalante-García, Alkali-activated slag-metakaolin pastes: strength structural and microstructural characterization, Sust. Cem-Based Mater. 2 (2013) 111–127.
[26] A. Palomo, M.T. Blanco-Varela, M.L. Granizo, F. Puertas, T. Vazquez, M.W. Grutzeck, Chemical stability of cementitious materials based on metakaolin, Cem. Concr. Res. 29 (1999) 997–1004.
[27] J. Davidovits, 30 years of successes and failures in geopolymer applications. Market trends and potential breakthroughs, in: Y. Ref (Ed.), Geopolymer 2002 Conference, Geopolymer Institute, Saint-Quentin, France, Melbourne, Australia, 2002.
[28] B.B. Sabir, S. Wild, J. Bai, Metakaolin and calcined clays as pozzolans for concrete: a review, Cem. Concr. Compos. 23 (2001) 441–454.
[29] K. Christina Yip, L. John Provis, C. Grant Lukey, S.J. Jannie van Deventer, Carbonate mineral addition to metakaolin-based geopolymers, Cem. Concr. Res. 30 (2008) 979–985.

[30] Debabrata. Dutta, Somnath. Ghosh, Effect of lime stone dust on geopolymerisation and geopolymeric structure, Intern. J. Emer. Tech. Adv. Eng. 11 (2012) 757–763.
[31] ASTM C109M, Standard test method for compressive strength of hydraulic cement mortars. 2007.
[32] ASTM C1403. Standard test method for rate of water absorption of masonry mortars. 2013.
[33] ASTM C191, 2013. Standard Test Methods for Time of Setting of Hydraulic Cement by Vicat Needle.
[34] Jessica Camiletti, Ahmed Soliman, Moncef Nehdi, Effect of nano-calcium carbonate on early-age properties of ultrahigh-performance concrete, Magaz. Concr. Res. 65 (5) (2013) 297–307.
[35] P. Duxson, J.L. Provis, J.S.J. van Deventer, Geopolymers: Structures, processing, properties and industrial applications, Woodhead Publishing, Abingdon UK, 2009.
[36] W. Mozgawa, J. Deja, Spectroscopic studies of alkaline activated slag geopolymers, Mol. Struct. 924–926 (2009) 434–441.
[37] Fei Jin, Gu Kai, Abir Al-Tabbaa, Strength and drying shrinkage of reactive MgO modified alkali-activated slag paste, Constr. Buil. Mater. 51 (2014) 395–404.